Turbulence, Heat and Mass Transfer 5
K. Hanjalić, Y. Nagano and S. Jakirlić (Editors)

DNS and Wavelet Analysis of a Turbulent Channel Flow Rotating about the Streamwise Direction

T. Weller[1], K. Schneider[2], M. Oberlack[1], and M. Farge[3]

[1]*Department of Mechanical Engineering, Chair of Fluid Dynamics, Technische Universität Darmstadt, Petersenstr. 13, 64287 Darmstadt, Germany, weller@fdy.tu-darmstadt.de, office@fdy.tu-darmstadt.de*

[2]*Laboratoire de Modélisation et Simulation Numérique en Mécanique, CNRS et Universités d'Aix-Marseille & CMI, Université de Provence, 39 rue Frédéric Joliot-Curie, 13453 Marseille, France, kschneid@cmi.univ-mrs.fr*

[3]*Laboratoire de Météorologie Dynamique, CNRS et Ecole Normale Supérieure, 24 rue Lhomond, 75231 Paris, France, farge@lmd.ens.fr*

Abstract — In this contribution a study of a turbulent channel flow rotating about the streamwise direction is presented by using direct numerical simulation (DNS). The theory giving a theoretical basis for the mean flow is based on the investigations of [9] employing symmetry group theory. It was found both in DNS and in the theory that a cross flow in the spanwise direction is induced. Statistical evaluations have shown that all six components of the Reynolds stress tensor are non-zero. A series of DNS has been conducted at Reynolds number $Re_\tau = 180$ for both the non-rotating case and different rotation numbers up to $Ro = 20$ to examine the effects of rotation. Further a wavelet analysis has been performed for selected data sets computations to identify and extract coherent vorticities.

1. Introduction

Rotating turbulent flows play an increasing role in engineering applications such as in gas turbine blade passages, pumps and rotating heat exchangers to name only a few. In these cases secondary flows are induced caused by centrifugal or Coriolis forces.

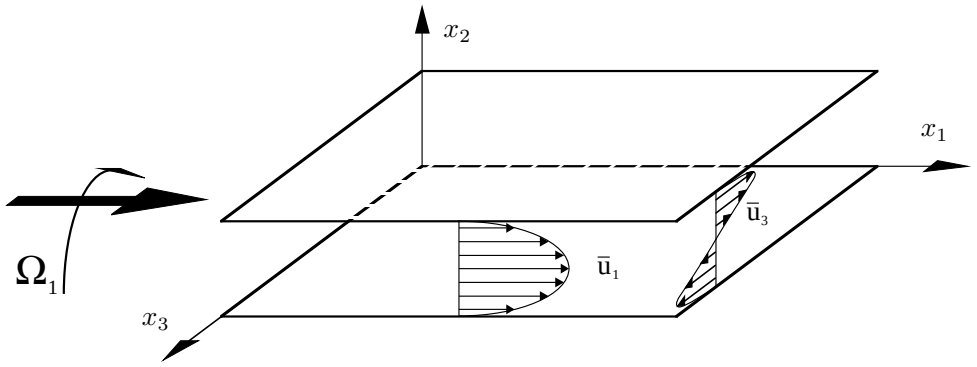

Figure 1: Sketch of the flow geometry of a turbulent channel flow rotating about the mean flow direction

Investigations in [9] using symmetry theory showed that there is a new turbulent scaling law related to the turbulent channel flow rotating about the mean flow direction. Figure 1 depicts the flow geometry. The flow has several common features with the classical rotating channel flow rotating about the spanwise direction [6] but also has some different characteristics. The induction of a mean velocity in x_3-direction [10] is the most obvious difference compared to the classical case. This cross flow can be deduced by investigating the mean momentum equation and the Reynolds stress transport equation. Statistical evaluations have shown that all six components of the Reynolds stress tensor are non-zero.
In this paper the results of a DNS at Reynolds numbers $Re_\tau = 180$ first for the non-rotating case and second for different rotation rates up to Ro=20 are presented. The main objective of the present paper is to analyze the influence of different rotation rates compared to the non-rotating case. Further a wavelet analysis by using the coherent vortex extraction (CVE) method has been performed for same selected computations to identify and extract coherent vorticities.

2. Direct Numerical Simulation

2.1. Numerical Method and Computations

The numerical technique which was chosen is a standard spectral method with Fourier decomposition in streamwise and spanwise direction as well as Chebyshev decomposition in wall-normal direction. The numerical code for channel flow was developed at KTH/Stockholm [8]. Additional features such as the streamwise rotation and statistics were added during the project. All flow quantities are non-dimensionalized by $h/2$ and u_{cl} where h is the channel width and u_{cl} is the center line velocity of the flow field. The boundary conditions are non-slip at $x_2 = \pm 1$ and periodic in x_1- and x_3-direction. For all computations the pressure-gradient is kept constant. Further details on the numerical scheme may be obtained from [8].
After the simulations were finalized all flow quantities were normalized on the friction velocity u_τ. So the Reynolds number is defined by

$$Re_\tau = \frac{h u_\tau}{2\nu} \tag{1}$$

and the rotation number as

$$Ro = \frac{\Omega h}{u_\tau}. \tag{2}$$

Table 1 gives an overview on the different computations, the flow domain and corresponding grid points. All presented results for the non-rotating case $Ro = 0$ are in good agreement with the data from Kim et. al [7].
A general problem with the DNS of rotating flows is that they require rather long integration times to obtain stable statistics i.e. meaningful results especially for the statistical quantities such as $\overline{u_i' u_j'}$ (see [11]). All computations in table 1 were run for $10000\frac{h/2}{u_{cl}}$ time units and the statistics accumulation was performed for the last 5000 time units.

Table 1: Computations at Reynolds number $Re_\tau = 180$

N	Ro	Box($x_1 \times x_2 \times x_3$)	Grid($x_1 \times x_2 \times x_3$)	Grid points
1	0	$8\pi \times 2 \times 4\pi$	$128 \times 129 \times 128$	2.4 Mio
2	1	$8\pi \times 2 \times 4\pi$	$256 \times 129 \times 128$	4.2 Mio
3	3.2	$8\pi \times 2 \times 4\pi$	$256 \times 129 \times 128$	4.2 Mio
4	5.2	$8\pi \times 2 \times 4\pi$	$256 \times 129 \times 128$	4.2 Mio
5	10	$8\pi \times 2 \times 4\pi$	$256 \times 129 \times 128$	4.2 Mio
6	14	$8\pi \times 2 \times 4\pi$	$256 \times 129 \times 128$	4.2 Mio
7	20	$8\pi \times 2 \times 4\pi$	$256 \times 129 \times 128$	4.2 Mio

2.2. Main Profiles and Reynolds Stress Tensor

Figure 2 shows the streamwise mean velocity profiles at different rotation rates. The profiles decrease invariably with increasing rotation numbers. The profiles all decrease evenly but beetween $Ro = 5.2$ and $Ro = 10$ the peeks of the profiles decreases from $\bar{u}_3^+ = 16.94$ down to $\bar{u}_3^+ = 13.98$. It concerns about a very strong decrease.
In figure 3 the spanwise mean velocity profiles at different rotation rates are displayed. The predicted cross flow from group theory [9] could also be verified in the DNS. In general the spanwise velocity profiles are skew-symmetric about the centerline. Furthermore some new interesting effects were found. At first the averaged profile $\bar{u}_3$ of the cross flow is formed like a 'S' that means it exhibits a triple zero-crossing and secondly the *reverse effect*. Reverse effect means that for small rotation rates up to Ro=10 the spanwise mean velocity profiles increase and at rotation number $Ro = 14$ this effect appears to reverse. It is important to note that the *reverse effect* takes place nearly in the same interval of the rotation rates where the streamwise mean velocity profiles highly decrease. It seems that in this region a kind of saturation is reached.

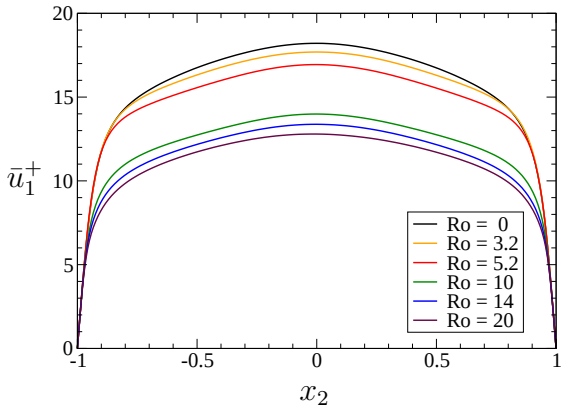

Figure 2: Streamwise mean velocity profiles at different rotation rates.

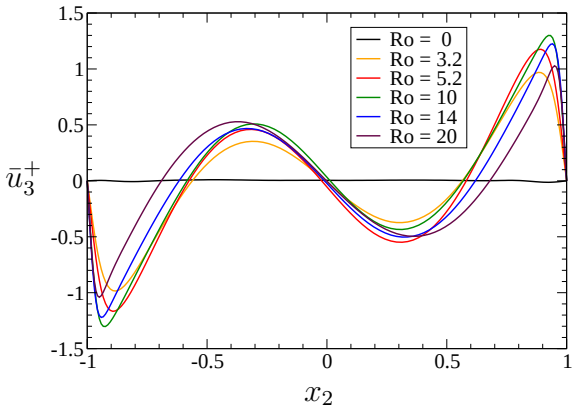

Figure 3: Spanwise mean velocity profiles at different rotation rates.

From the statistical one-point quantities, only the Reynolds stress tensor is depicted. In the figures 4 - 9 the six components are shown for five selected rotation numbers $Ro = (0, 3.2, 10, 14, 20)$. All stresses are nondimensionalized with u_τ. As predicted from the Lie group analysis [9] the DNS shows also in contrast to the non-rotating case that all six components of the Reynolds

stress tensor are non zero. All statistical curves are symmetric or skew-symmetric about the centerline. The stresses $\overline{u_1'u_1'}$ and $\overline{u_1'u_3'}$ decrease at higher rotation, whereas $\overline{u_2'u_2'}$, $\overline{u_3'u_3'}$ and $\overline{u_1'u_3'}$ increase. The shear stress $\overline{u_1'u_2'}$ is nearly similar for all rotation rates. For the shear stress $\overline{u_2'u_3'}$ the same *reverse effect* such as for the spanwise mean velocity profiles is noticeable. They increase for small rotation rates and reverse exactly at the same rotation rate $Ro = 14$ just as in the spanwise mean profiles.

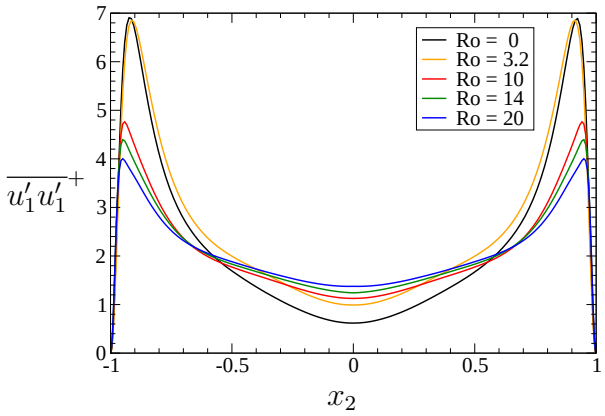

Figure 4: Reynolds normal stresses $\overline{u_1'u_1'}$.

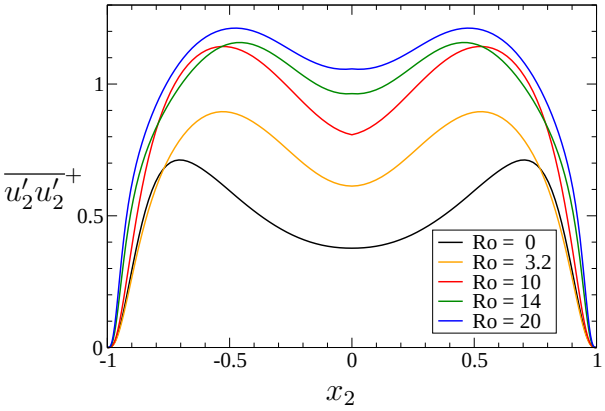

Figure 5: Reynolds normal stresses $\overline{u_2'u_2'}$.

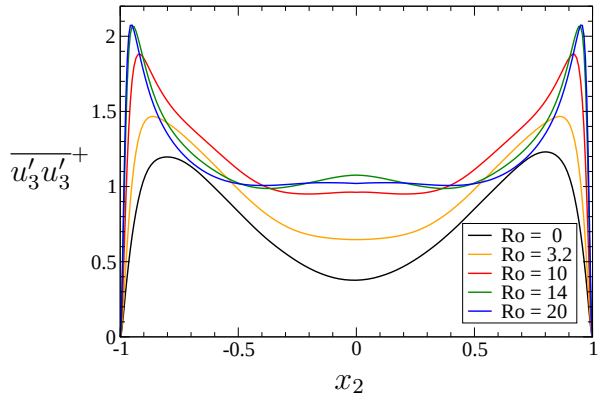

Figure 6: Reynolds normal stresses $\overline{u_3'u_3'}$.

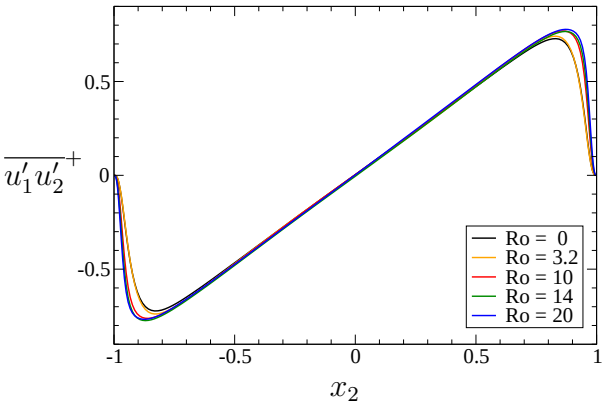

Figure 7: Reynolds shear stresses $\overline{u_1'u_2'}$.

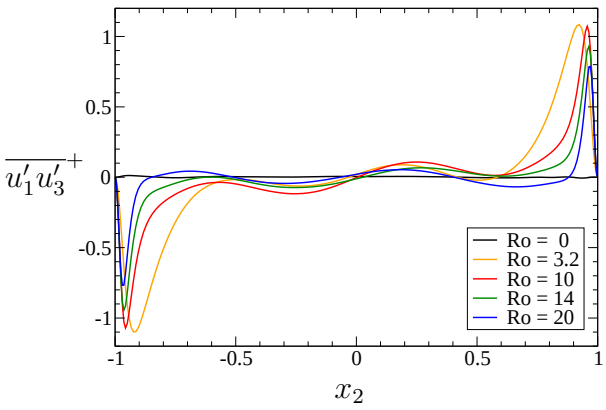

Figure 8: Reynolds shear stresses $\overline{u_1'u_3'}$.

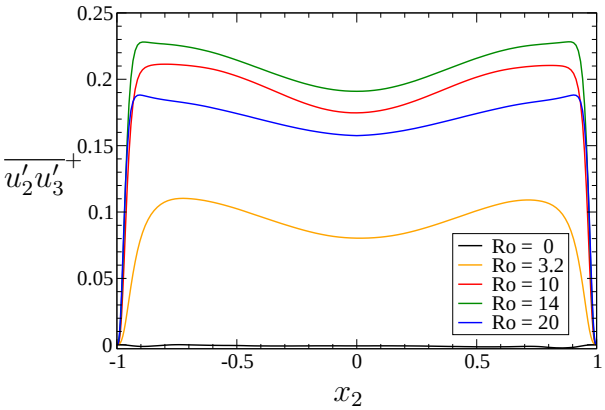

Figure 9: Reynolds shear stresses $\overline{u_2'u_3'}$.

2.3. Isosurface of the velocity field

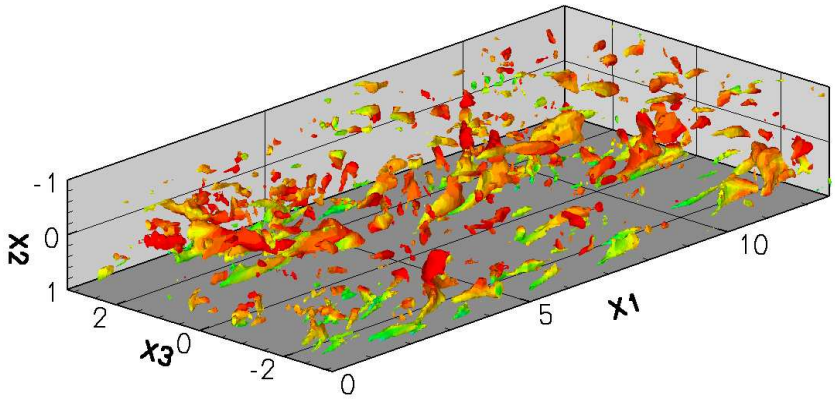

Figure 10: u_2-isosurface at Ro=0

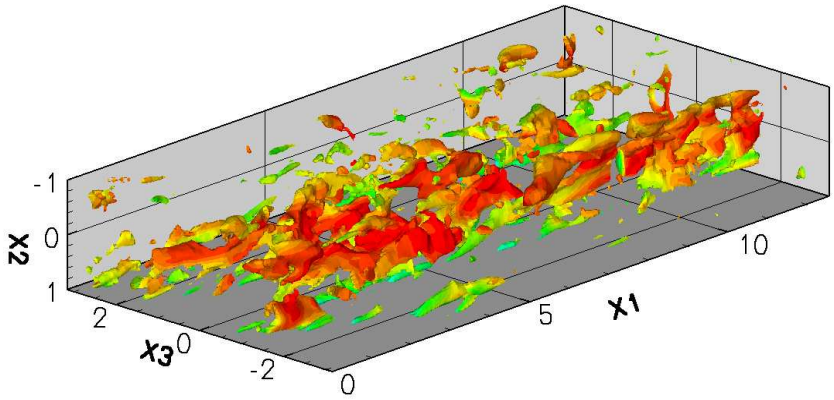

Figure 11: u_2-isosurface at Ro=5.2

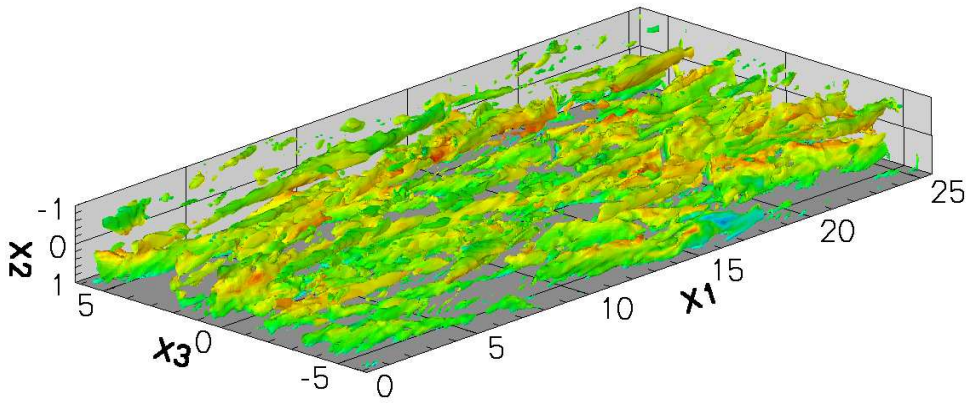

Figure 12: u_2-isosurface at Ro=20

In figures 10 - 12 the isosurfaces of the wall-normal velocity field are visualized at the instantaneous time unit $t \simeq 10000\frac{h/2}{u_c l}$ for both the non-rotating case and for two different rotation rates,

for a small $Ro = 5.2$ and a higher rotation rate $Ro = 20$. To compare the figure, the same value for the isosurfaces is used. For the non-rotating case the velocity field is very disordered, at $Ro = 5.2$ a few small structures are visible and at $Ro = 20$ a lot of large turbulent structures are formed. Apparently with increasing rotation number increasingly elongated turbulent structures are formed.

2.4. x_1x_3-slices of the vorticity field

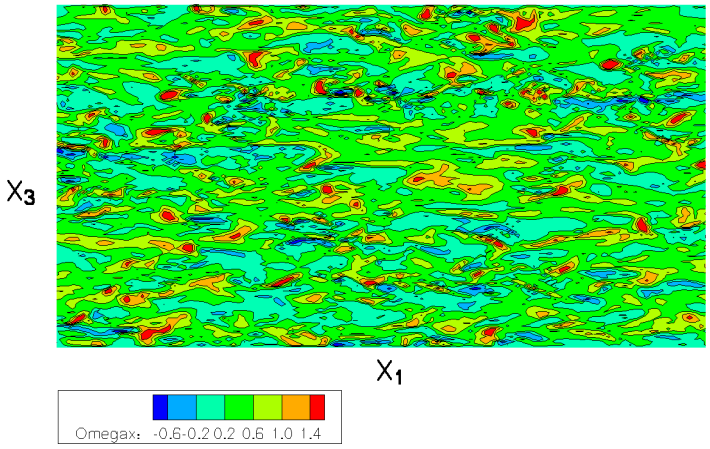

Figure 13: x_1x_3-slice ($x_2 = 0.9$, near the wall) of the streamwise vorticity field at $Ro = 0$.

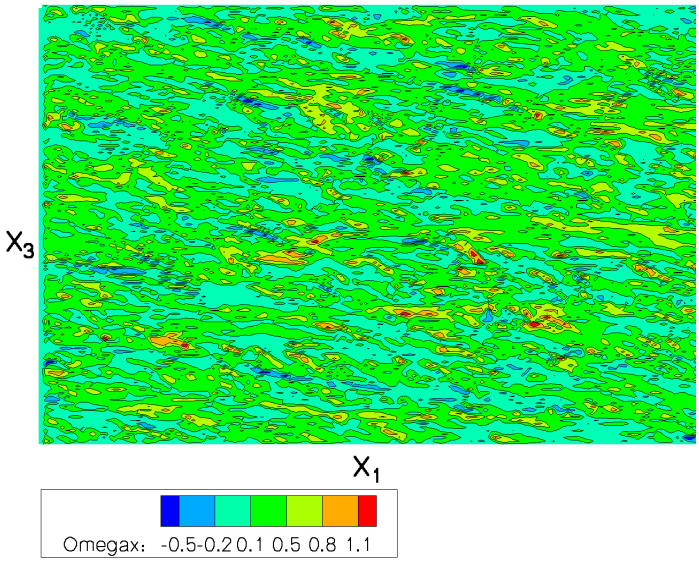

Figure 14: x_1x_3-slice ($x_2 = 0.9$, near the wall) of the streamwise vorticity field at $Ro = 20$.

The figures 13 and 14 show x_1x_3-slices for $x_2 = 0.9$ (near the wall) of the streamwise vorticity field at an instantaneous time unit $t \simeq 10000\frac{h/2}{u_{cl}}$ for two different cases. e.g. the non-rotating case and second a rotating case at rotation number $Ro = 20$. In the non-rotating some straight vorticity structures are observed.

For the rotating case two effects are to mention. One effect is that the number of vorticities is increasing but at the same time they become smaller. The other effect is that caused by the rotation the structures are diverted from the streamwise direction which was also to expected from the cross flow. Both is clearly visible in figures 14.

3. Wavelet Analysis

3.1. Wavelet method for coherent vortex extraction (CVE)

An orthogonal wavelet-based method to extract coherent vortices from 3D turbulent flow is proposed by Farge et. al. [5]. Considered is the vorticity field $\omega_i = \nabla \times u_i$ at resolution $N = 2^{3J}$, where N is the number of grid points and J the corresponding number of octaves. Each component is developed into an orthogonal wavelet series, from the largest scale $l_{max} = 2^0$ to the smallest scale $l_{min} = 2^{1-J}$, using as 3D multi-resolution analysis (MRA). For more details on the MRA see [1, 4].
The extraction algorithm can be summarized as follows:

1. Given ω_i, sampled on a grid (x_i, y_j, z_k) for $i, j, k = 0, N-1$ and the total enstrophy $Z = \frac{1}{2}\int |\omega_i|^2 dx$.

2. Perform the 3D wavelet decomposition by applying the Fast Wavelet Transform (FWT) to each component of ω_i to obtain the three components of $\tilde{\omega}^{\mu}_{j,i_x,i_y,i_z}$ for $j = 0, J-1, i_x, i_y, i_z = 0, 2^{J-1}$, and $\mu = 1, ..., 7$.

3. Compute the thresholding, where Z is the Enstrophy and N the number of grid points,

$$T = \sqrt{\frac{4Z}{3}\ln N} \tag{3}$$

   and split the coefficients $\tilde{\omega}_i$ into

$$\tilde{\omega}_{i,coh} = \begin{cases} \tilde{\omega}_i & \text{for} \quad |\tilde{\omega}_i| \geq T, \\ 0 & \text{for} \quad |\tilde{\omega}_i| < T \end{cases} \quad \text{and} \quad \tilde{\omega}_{i,inc} = \begin{cases} \tilde{\omega}_i & \text{for} \quad |\tilde{\omega}_i| < T, \\ 0 & \text{for} \quad |\tilde{\omega}_i| \geq T \end{cases} \tag{4}$$

4. Perform the 3D wavelet reconstruction by applying the inverse FWT to compute $\omega_{i,coh}$ and $\omega_{i,inc}$ from $\tilde{\omega}_{i,coh}$ and $\tilde{\omega}_{i,inc}$, where *coh* and *inc* corresponds to coherent and incoherent.

3.2. Application to turbulent rotating channel flow and results

In the present work the CVE method was conducted for six selected cases of table 1 at Reynolds number $Re_\tau = 180$. At first for the non-rotating case and further for the rotating cases at five different rotation rates $Ro = 1, 3.2, 5.2, 10$ and 20.
In this study orthogonal *Coiflet 12* wavelets are used which are of order $c = 12$ and having four vanishing moments. c denotes the length of the associated quadratic mirror filter [1, 4]. The choice of the threshold (equation 3) is based on Donohos theorems [1, 3]. For each wavelet analysis one Donoho iteration was conducted.
Because the orthogonal wavelet decomposition requires that the number of grid points is a power of two in each direction, the vorticity fields have to be interpolated. The main problem is the Chebychev decomposition in the wall-normal direction used in the spectral code of the DNS. It makes a grid of a power of two impossible.

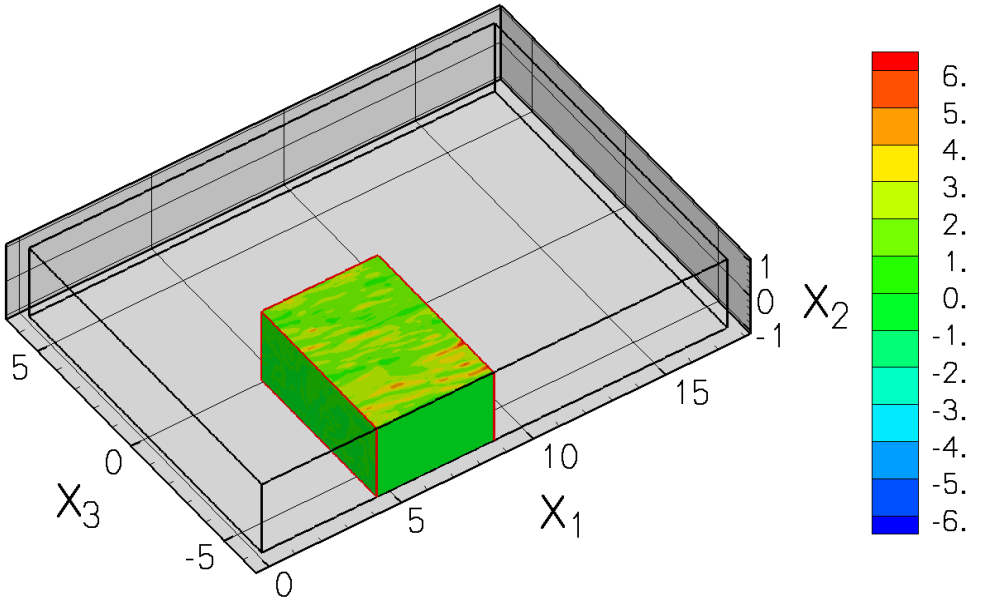

Figure 15: Sketch of the channel to illustrate the subzone which is visualized in fig. 16

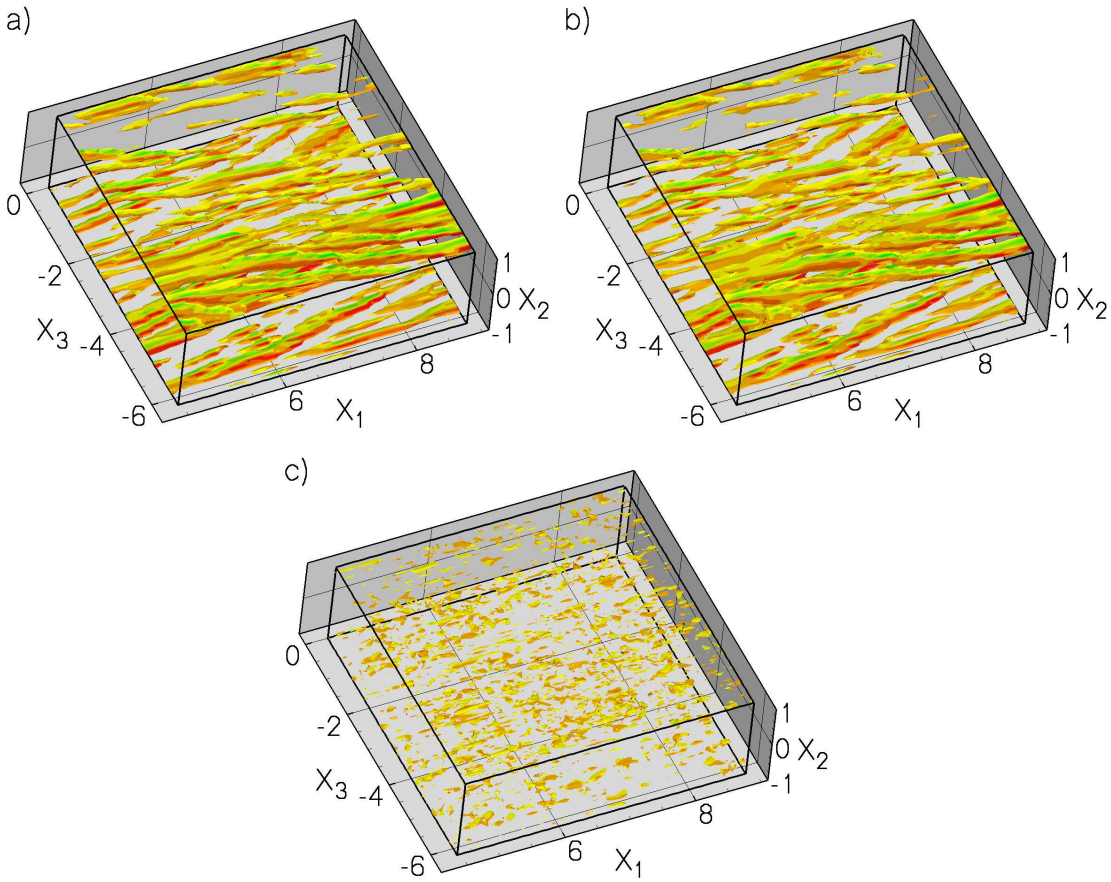

Figure 16: Isosurface of the streamwise vorticity field at $Ro = 10$: a) total subzone, b) coherent component: 3.61% of the wavelet coefficients and c) incoherent component: 96.39% of the wavelet coefficients. For all figures the colormap shown in fig. 15 is used.

The utilized method for the interpolation is the *inverse distance method*. For the non-rotating case the vorticity field was interpolated in physical space from a grid of $(128 \times 129 \times 128)$ to $(128 \times 128 \times 128)$ and for all other cases from $(256 \times 129 \times 128)$ to $(256 \times 128 \times 128)$.
In figure 15 a sketch of the channel to illustrate the subzone which is visualized in fig. 16 is shown. Although the CVE was done for the whole channel for the visualizations in figure 16 a subzone is selected to have a better zoom of the vorticities. For the subzone a quarter of the streamwise (64-128), half of the spanwise (1-64) and all of the wall-normal grid points (1-128) were selected. Figure 16 shows the streamwise isosurfaces of a) the total subzone, b)

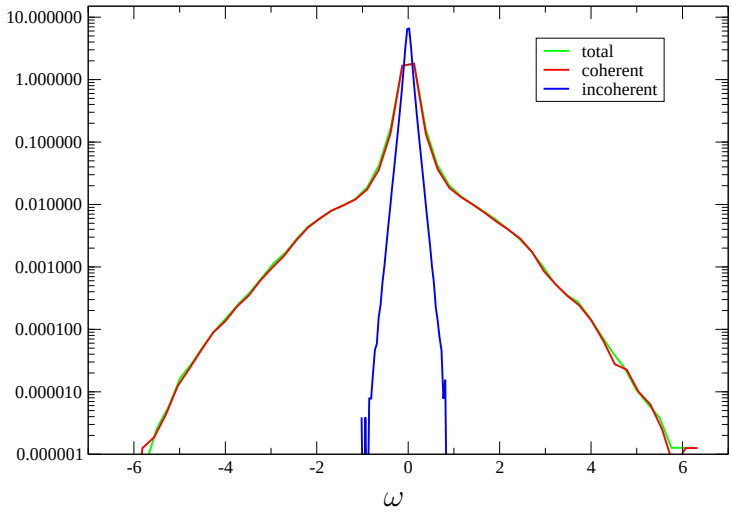

Figure 17: Normalized PDF of vorticity field for the non-rotating case.

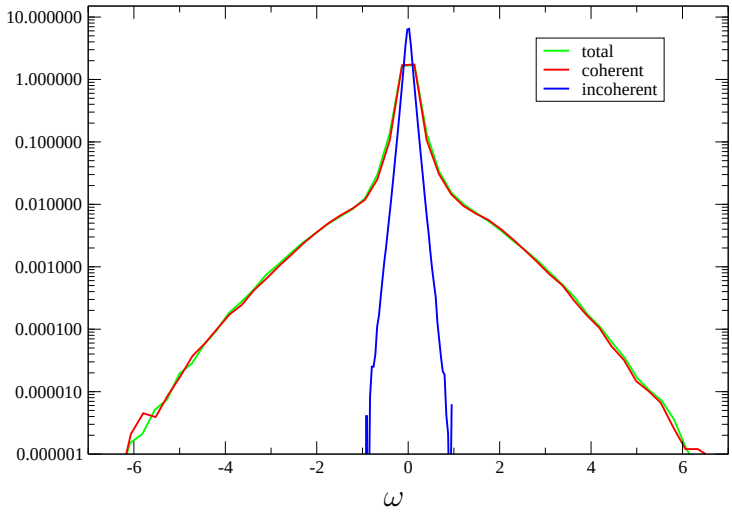

Figure 18: Normalized PDF of vorticity field at rotation rate $Ro = 10$.

the coherent part and c) the incoherent part of an instantinous 3D vorticity field at $Ro = 10$ and Reynolds number $Re_\tau = 180$. The streamwise component was chosen because it is the dominant part of $|\omega|$. The isosurfaces of the total subzone and the coherent part were plotted for the same values $\omega_{x_1} = \pm 1.9$ and the incoherent part for $\omega_{x_1} = \pm 0.28$. Only to mention for all figures the same colormap is used (shown in fig. 15). Interesting enough we found that few

Table 2: Compression rate and Enstrophy of vorticity at Reynolds number $Re_\tau = 180$

	Compression rate		Enstrophy	
Ro	coherent[%]	incoherent[%]	coherent[%]	incoherent[%]
0	3.41	96.59	94.85	5.15
1	3.24	96.76	96.54	3.46
3.2	3.14	96.86	97.07	2.93
5.2	3.12	96.88	97.22	2.78
10	3.61	96.39	93.53	6.47
20	3.60	96.40	94.18	5.82

Table 3: Skewness and flatness of vorticity at Reynolds number $Re_\tau = 180$

	Skewness			Flatness		
Ro	total	coherent	incoherent	total	coherent	incoherent
0	-0.090	-0.07	-0.015	33.708	36.184	6.719
10	0.298	0.342	-0.018	43.618	47.773	6.262

strong wavelet coefficients (3.61%) represent the coherent vortices of the flow (Fig. 16b)) while the remaining weak coefficients correspond to the incoherent background flow (Fig. 16c)).

In table 2 the rates of the coherent and incoherent components of the compression rate and the enstrophy are given for all rotation rates mentioned above. Compared to the non-rotating case the compression for the coherent structures is decreasing for small rotation rates up to $Ro = 5.2$. At $Ro = 10$ the compression rate appears to revers it increases suddenly up to 3.61%. Concerning enstrophy the values are inversely to the compression rate. For small rotation rates the coherent part increases compared to the non-rotating case and at $Ro = 10$ the enstrophy decreases down to 94.18%.

Important to note that this *reverse effect* was also found for higher rotation rates in the DNS for the cross flow $\bar{u}_3$ and the shear stress $\overline{u_2' u_3'}$. For $Ro = 10$ the streamwise mean velocity profile $\bar{u}_1$ exhibits a strong decrease. The *reverse effect* in both the compression rate and the enstrophy confirms the assumption of a saturation.

In figures 17 and 18 the PDFs of vorticity for the total, coherent and incoherent fields are visualized for the non-rotating case and at rotation number $Ro = 10$. Both figures are very similar and it appears there is no noticeable influence due to rotation. However in table 3 the modulus of skewness and flatness of vorticity is calculated for the same components and data sets. The skewness for the total and coherent field at rotation number $Ro = 10$ is much greater than for the non-rotating case and at the same time the sign is changing. The flatness of the total and coherent field increases approximately 23% at rotation number $Ro = 10$. It seems that also a kind of influence is given due the rotation which is not directly visible in the PDFs.

4. Conclusions

The influence of different rotation rates of a rotating turbulent channel at Reynolds number $Re_\tau = 180$ is examined. The results of the DNS agree with the results of the symmetry theory. Not only the predicted cross flow could be verified in the DNS at different rotation rates but

also some new properties were detected. At first the averaged profiles $\bar{u}_3$ of the cross flow are formed like a 'S' that means it exhibits a triple zero-crossing and secondly the *reverse effect* for the cross flow $\bar{u}_3$ and the shear stress $\overline{u_2' u_3'}$ which starts at $Ro = 14$. For the same rotation number the streamwise mean velocity profile decreases highly. Further for increasing rotation rates increasingly elongated turbulent structures are formed in the isosurface of the wall-normal velocity field. Another effect is that caused by the rotation the turbulent structures of the vorticity field are diverted from the streamwise direction.
Further the CVE was conducted for six selected data sets. We found that for all data sets a few strong wavelet coefficients represent the coherent vortices of the flow while the remaining weak coefficients correspond to the incoherent background flow. In both the compression rate and the enstrophy a similar *reverse effect* compared to the DNS was found, it seems to confirm the assumption of a saturation. The influence of rotation is not directly visible in the PDFs but it can be detected by the use of statistics calculations e.g skewness and flatness.
Future investigations are planned, especially simulations and CVEs at higher Reynolds numbers.

References

1. I. Daubechies. *Ten Lectures on Wavelets*. SIAM, CBMS-NSF Conference Series in Applied Mathematics., vol. 61, Philadephia, 1992.
2. D. Donoho. Unconditional bases are optimal bases for data compression and statistical estimation. *Appl. Comput. Harmon Anal.*, 1:100–115, 1993.
3. D. Donoho and I. Johnstone. Ideal spatial adaption via wavelets shrinkage. *Biometrica*, 81:425–455, 1993.
4. M. Farge. Wavelet transforms and their application to turbulence. *Annu. Rev. of Fluid Mech.*, 24:395–457, 1992.
5. M. Farge, G. Pellegrino and K. Schneider. Coherent Vortex Extraction in 3D Turbulent Flows using orthogonal wavelets. *Phys. Rev. Lett.*, 87(5):45011–45014, 2001.
6. P.J. Johnston, R.M. Halleen and D.K. Lazius. Effects of spanwise rotation on the structure of two-dimensional fully developed turbulent channel flow. *J. Fluid Mech.*, 56:533–557, 1972.
7. J. Kim, P. Moin, and R. Moser. Turbulence statistics in fully developed channel flow at low Reynolds number. *J. Fluid Mech.*, 177:133–166, 1987.
8. A. Lundbladh, D. Henningson and A. Johanson. An efficient spectral integration method for the solution of the Navier-Stokes equations. *FFA-TN 1992-28, Aeronautical Research Institute of Sweden, Bromma*, 1992.
9. M. Oberlack, W. Cabot, B. A. Pettersson Reif, T. Weller: Group analysis, DNS and Modeling of a Turbulent Channel Flow with Streamwise Rotation, *accepted for publication in J. Fluid Mech*, 2006.
10. M. Oberlack A unified approach for symmetries in plane parallel turbulent shear flows. *J. Fluid Mech.*, 427:299–328, 2001.
11. T. Weller, I. Recktenwald, M. Oberlack and W. Schröder. DNS and Experiment of a Turbulent Channel Flow with Streamwise Rotation - Study of the Cross Flow Phenomena. In *Proc. in Appl. Math. and Mech. (PAMM)*, vol.5, pp.569-570, 2005.
12. T. Weller and M. Oberlack. DNS of a Turbulent Channel Flow with Streamwise Rotation - Investigation on the Cross Flow Phenomena. *Accepted for publication in Proc. of DLES6*, 2005.